CHAPTER 1

INTRODUCTION

Heating and cooling of fluids flowing inside conduits are among the most important heat transfer processes in engineering. The design and analysis of heat exchangers require a knowledge of the heat transfer coefficient between the wall of the conduit and the fluid flowing inside it. The sizes of boilers, economizers, super heaters, and pre heaters depend largely on the heat transfer coefficient between the inner surface of the tubes and the fluid. Also, in the design of air-conditioning and refrigeration equipment, it is necessary to evaluate heat transfer coefficients for fluids flowing inside ducts. Once the heat transfer coefficient for a given geometry and specified flow conditions is known, the rate of heat transfer at the prevailing temperature difference can be calculated from the equation [1].

$$q_c = \bar{h}_c A(T_{surface} - T_{fluid})$$

1.1 Heat Transfer Enhancement Techniques

The improvements in the efficiency of heat exchangers can lead to substantial cost, space and materials savings. Therefore, considerable research work has been done in the past to seek effective ways to increase the efficiency of heat exchangers. The referred investigations include the selection of working fluids with high thermal conductivity, selection of their flow arrangement and high effective heat transfer surfaces made from high-conductivity materials. For both single-phase and two-phase heat transfer, effective heat transfer enhancement techniques have been reported. However, in the present work only the single-phase forced convection enhancement techniques have been considered. The

heat transfer enhancement methods may be grouped as passive, active and compound enhancement methods.

1.1.1 Active Techniques

The basis of any active heat transfer enhancement technique lies in the utilization of some external power in order to permit the mixing of working fluids, the rotation of heat transfer surfaces, the vibration of heat transfer surfaces or of the working fluids, and the generation of electrostatic fields. Generally, active heat transfer enhancement methods have not been well established in industrial applications owing to the capital and operating costs and problems associated with vibration or acoustic noise.

1.1.2 Passive Techniques

The major heat transfer enhancement techniques that have found widely spread commercial application are those which possess heat transfer enhancement elements. All passive techniques aim for the same, namely to achieve higher values of the product of heat transfer coefficient and heat transfer surface area [2]. These techniques generally use surface or geometrical modifications to the flow channel by incorporating inserts or additional devices. These techniques do not require any direct input of external power; rather they use it from the system itself which ultimately leads to an increase in fluid pressure drop [3].

1.1.3 Compound Techniques

When any two or more techniques employed simultaneously to obtain enhancement in heat transfer that is greater than that produced by either of them when used individually, is termed as compound enhancement [3].

1.2 Compact Heat Exchanger

Compared to shell-and-tube heat exchangers, compact heat exchangers are characterized by a large heat transfer surface area per unit volume of the exchanger, resulting in reduced space, weight, energy requirements and cost, as well as improved process design and plant layout and processing conditions. A gas-to-fluid exchanger is referred to as a compact heat exchanger if it incorporates a heat transfer surface having a surface area density β greater than about $700m^2/m^3$ or a hydraulic diameter $D_h \leq 6mm$ for operating in a gas stream and $400m^2/m^3$ or higher for operating in a liquid stream. In contrast, a typical process industry shell and-tube heat exchanger has a surface area density of less than $100m^2/m^3$ on one fluid side with plain tubes, and two to three times greater than that with high-fin-density low-finned tubing. A typical plate heat exchanger has about twice the average heat transfer coefficient h on one fluid side or the average overall heat transfer coefficient U than that for a shell and tube exchanger for water/water applications. A compact heat exchanger is not necessarily of small bulk and mass. However, if it did not incorporate a surface of high-surface area density, it would be much more bulky and massive [4].

1.3 Problem Statement

Lately compact heat exchangers (CHE) have been subject of extensive research, because of their importance in a wide variety of engineering applications. Fins are playing a vital role in such equipments to enhance their performance. One of the most common designs in these applications use an enclosed pin fin heat exchanger duct flow configuration with pins of round cross section .The results of the previous studies indicate that the drop shaped pin fins yield a considerable improvement in heat transfer and pressure drop characteristics compared to circular pin fins for the same heat transfer wetted surface area. So the question what is the optimum drop shaped dimension that

maximizes the heat transfer and minimizes the pressure drop across the heat exchanger.

1.4 Objectives of the Study

The aim of this thesis is to study one of the active heat transfer enhancement devices for the heat exchanger. In order to achieve this aim, the following objectives were set out:

1. To simulate the heat exchanger of the different drop shaped fin dimension having same wetted surface area for different Reynolds number in the range of 5000 to 20000 with interval of 2500.
2. To compare the performance of the different cases to select the optimum drop shaped fin dimension based on maximum heat transfer and minimum pressure drop.

1.5 Scope of the work

The aim of this thesis is to conduct a numerical study using ANSYS FLUENT to select the optimum pin dimension considering maximum heat transfer and minimum pressure drop across the heat exchanger. This aim can be achieved by the following steps:

1. Study the fundamental of pin fin heat exchangers and their applications.
2. Validation, by simulating pin fin model which was already tested experimentally and compare the numerical results with the experimental data.
3. Simulation of drop shaped pin fin heat exchanger of four different fins dimension that have typical heat transfer wetted surface area.

4. Analysis of the results for each model to select the optimum drop shaped fin dimension that maximize the heat transfer and minimize the pressure drop across the heat exchanger.

CHAPTER 2

LITERATURE REVIEW

Heat transfer from pin fin arrays is a subject of high importance with many engineering applications. These applications range from compact heat exchangers, boilers for steam turbines, to the convective internal cooling of gas turbine air foils. Due to the complex nature of the flow fields, no analytical solution exists that can accurately predict pin fin array heat transfer.

This section presents a brief look at the research that has been conducted prior to the writing of this report.

C. L. Chapman and Seri Lee [5] carried out comparative thermal tests using aluminum heat sinks made with extruded fin, cross-cut rectangular pins and elliptical shaped pins in low air flow environments. They developed an elliptical pin fin heat sink with specific design parameters, maintaining large exposed surface area for heat transfer and minimizing vortex flow by incorporating an airfoil design. The approach taken in the paper was to compare this elliptical shaped heat sink with a conventional extruded fin heat sink of equal volume. They found that there was 40% more air flowing through the rectangular pin design, yet the thermal resistances were virtually equal and the elliptical pin fin enhanced the heat transfer. These results were in correlation with the basis of the elliptical pin fin design considerations i.e. vortex flow is reduced and boundary layer effects are eliminated. Also surprisingly they found that extruded straight design performed significantly better than either of the two other designs over the flow range which they examined there. Ambeprasad.S.Kushwaha and Ravindra Kirar [6] dealt with the comparative study of heat sink having fins of various profiles namely Rectangular, Trapezoidal and Parabolic. For the purpose of study heat sink is modeled by

using the optimal geometric parameter such as fin height, fin thickness, base height, fin pitch as 48 mm, 1.6 mm, 8 mm, 2 mm and after that simulation is done at different heat load of 50W, 75W, 100W and with a air flow at 15 CFM and air inlet temperature is taken as 295 K.. The result obtained taking into consideration only the thermal performance. Yoav Peles, et.al [7] investigated heat transfer and pressure drop phenomena over a bank of micro pin fins. It has been found that very low thermal resistances are achievable using a pin fin heat sink. The thermal resistance values are comparable with the data obtained in microchannel convective flows. Michael E. Lyall [8] focused on but not limited to internal cooling of turbine airfoils using pin fins. This study examines heat transfer from a single row of circular pin fins with the row oriented perpendicular to the flow. The configurations studied have spanwise spacing to pin diameter ratios of two, four, and eight. Low aspect ratio pin fins were studied whereby the channel height to pin diameter was unity. The experiments are carried out for a Reynolds number range of 5000 to 30,000. Heat transfer measurements are taken on both the pin and on the endwall covering several pin diameters upstream and downstream of the pin row. The results show that the heat transfer augmentation relative to open channel flow is highest for the smallest spanwise spacing for the lowest Reynolds number flows. The results also indicate that the pin fin heat transfer is higher than on the endwall. Fengming Wang, et.al [9] conducted numerical and experimental study of the flow and heat transfer characteristics inside a rectangular channel embedded with pin fins. Several differently shaped pin fins (i.e., circular, elliptical, and drop-shaped) with the same cross-sectional areas were compared in a staggered arrangement. The result indicate that the more streamlined drop-shaped pin fins were better at delaying or suppressing separation of the flow passing through them, which decreased the aerodynamic penalty compared to circular pin fins. The heat transfer enhancement of the drop-shaped pin fins was less than that of the circular pin fins. So that in terms of specific performance parameters, drop-

shaped pin fins are a promising alternative configuration to circular pin fins. Hamid Nabati [10] presented the results of numerical study of heat transfer and pressure drop in a heat exchanger that is designed with different shape pin fins. Circular, Rectangular and drop-shaped pins configuration variations included changes in pin spacing, axial pitch and pin height ratio. Correlations for Nusselt number and friction factor were developed. The optimum drop shaped pin array was shown to match the heat transfer rates obtained by the optimum circular pin configuration while incurring less than one third the specific fluid friction power losses. Jihed Boulares [11] presented the results of a combined numerical and experimental study of heat transfer and pressure drop behavior in a CHE designed with drop-shaped pin fins. The results indicate that the drop shaped pin fins yield a considerable improvement in heat transfer compared to circular pin fins for the same pressure drop characteristics. This improvement is mainly due to the increased wetted surface area of the drop pins, and the delay in the flow separation as it passes the more streamlined drop shaped pin fins. Jeffrey W. Summers [12] concentrated on the empirical characterization of a staggered array pin fin compact heat exchanger placed in a modular, rectangular wind tunnel. A full analysis of the heat transfer and pressure drop behavior was conducted on various pin- fin shapes (Cylindrical , drop shaped), sizes, and configurations . The study was based on airflow over a range of low Reynolds numbers in the laminar and low turbulent flow, as well as higher turbulent flow regimes.

CHAPTER 3

NUMERICAL METHODS

Computational fluid dynamics or (CFD) is the analysis of systems involving fluid flow, heat transfer and associated phenomena such as chemical reactions by means of computer-based simulation. The technique is very powerful and spans a wide range of industrial and non-industrial application areas [13].

3.1 ANSYS FLUENT Solver

ANSYS Fluent software contains the broad physical modeling capabilities needed to model flow, turbulence, heat transfer, and reactions for industrial applications. Special models that give the software the ability to model in-cylinder combustion, aero acoustics, turbo machinery, and multiphase systems have served to broaden its reach.

ANSYS Fluent software is used as an integral part of the design and optimization phases of their product development. Advanced solver technology provides fast, accurate CFD results, flexible moving and deforming meshes, and superior parallel scalability. User-defined functions allow the implementation of new user models and the extensive customization of existing ones. The interactive solver setup, solution and post-processing capabilities of ANSYS Fluent make it easy to pause a calculation, examine results with integrated post-processing, change any setting, and then continue the calculation within a single application. Case and data files can be read into ANSYS CFD-Post for further

analysis with advanced post-processing tools and side-by-side comparison of different cases.

The integration of ANSYS Fluent into ANSYS Workbench provides users with superior bi-directional connections to all major CAD systems, powerful geometry modification and creation with ANSYS Design Modeler technology, and advanced meshing technologies in ANSYS Meshing. The platform also allows data and results to be shared between applications using an easy drag-and-drop transfer, for example, to use a fluid flow solution in the definition of a boundary load of a subsequent structural mechanics simulation.

The combination of these benefits with the extensive range of physical modeling capabilities and the fast, accurate CFD results that ANSYS Fluent software has to offer results in one of the most comprehensive software packages for CFD modeling available in the world today. A native two-way connection to ANSYS structural mechanics products allows capture of even the most complex fluid–structure interaction (FSI) problems in the same easy-to-use environment, saving the need to purchase, administer or run third-party coupling software. Other multiphysics connections include electromagnetic–fluid coupling [14].

3.2 The Finite Volume Method

Finite volume methods are a class of discretization schemes that have proven highly successful in approximating the solution of a wide variety of conservation law systems. They are extensively used in fluid mechanics, meteorology, electromagnetics, semi-conductor device simulation, and many other engineering areas governed by conservative systems that can be written in integral control volume form [15].

Let Φ be any dependent scalar variable. The transport equation of Φ reads

$$\frac{\partial}{\partial t}(\rho\Phi) + \frac{\partial}{\partial x_i}\left(\rho u_i \Phi - \Gamma_\Phi \frac{\partial \Phi}{\partial x_i}\right) = S_\Phi \qquad (3.1)$$

Defining the convective and diffusive flux as:

$$I_i = \rho u_i \Phi - \Gamma_\Phi \frac{\partial \Phi}{\partial x_i} \qquad (3.2)$$

For steady state the term involving time derivative vanishes. Using equation (3.1), equation (3.2) can be written as:

$$\frac{\partial I_i}{\partial x_i} = S_\Phi \qquad (3.3)$$

Integration of equation (3.3) over a control volume in the physical space, using Gauss' theorem

$$\int_V \frac{\partial I_i}{\partial x_i} dV = \int_A I_i \, A_i \qquad (3.4)$$

Yields

$$\int_A I_i \, A_i = \int_A S \, dV \qquad (3.5)$$

The integral above yields the discretized equation

$$\sum_{faces} (I_i A_i)_{faces} = S\delta V \qquad (3.6)$$

Equation (3.6) is rearranged using the differencing scheme for I_i to the standard form.

$$a_p \Phi_p = \sum_{N\,B} a_{N\,B} \, \Phi_{N\,B} + S\delta V \qquad (3.7)$$

Equation (3.1) is solved with the iterative methods to obtain the approximate solution of the transport equation (3.1).

3.3 The Differencing Schemes

The differencing scheme is introduced to calculate the convective and diffusive flux in-order to solve the discretized equation. In the collocated grid arrangements all the variables are stored at the nodes, while the fluxes are calculated at the faces of the control volumes. Interpolation function is needed to obtain the variables on the faces. This interpolation function is known as differencing scheme [16].

3.3.1 Quadratic Upwind Differencing Scheme, QUICK

Higher-order schemes involve more neighbour points and reduce the discretisation errors by bringing in a wider influence. Below the discussion in some detail of Leonard's QUICK scheme, which is the oldest of these higher order schemes.

The quadratic upstream interpolation for convective kinetics (QUICK) scheme of Leonard (1979) uses a three-point upstream-weighted quadratic interpolation for cell face values. The face value of Φ is obtained from a quadratic function passing through two bracketing nodes (on each side of the face) and a node on the upstream side, Figure (3.2) [13].

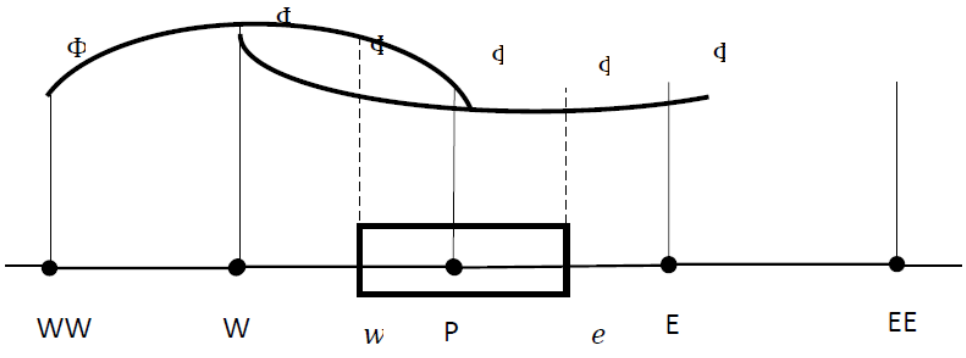

Figure (3.1): Quadratic profiles used in the QUICK scheme.

When $U_w > and\ U_e > 0$

Then

$$\Phi_{face} = \frac{6}{8}\Phi_{i-1} + \frac{3}{8}\Phi_i + \frac{1}{8}\Phi_{i-2}$$

$$\Phi_w = \frac{6}{8}\Phi_W + \frac{3}{8}\Phi_P + \frac{1}{8}\Phi_{WW}$$

$$\Phi_e = \frac{6}{8}\Phi_P + \frac{3}{8}\Phi_E + \frac{1}{8}\Phi_W$$

3.4 Turbulence

The Reynolds number of a flow gives a measure of the relative importance of inertia forces (associated with convective effects) and viscous forces. In experiments on fluid systems it is observed that at values below the so called critical Reynolds number Re_{crit} the flow is smooth and adjacent layers of fluid slide past each other in an orderly fashion. If the applied boundary conditions do not change with time the flow is steady. This regime is called laminar flow.

At values of the Reynolds number above Re_{crit} a complicated series of events takes place which eventually leads to a radical change of the flow character. In the final state the flow behavior is random and chaotic. The motion becomes intrinsically unsteady even with constant imposed boundary conditions. The velocity and all other flow properties vary in a random and chaotic way. This regime is called turbulent flow [13].

3.4.1 Turbulence Models

A turbulence model is a computational procedure to close the system of the mean flow equations. For a turbulence model to be useful in a general

purpose CFD code it must have wide applicability, be accurate, simple and economical to run [16]. According to Versteeg [13], the most common turbulence models are classified to:

- Classical models:
  1. Zero equation model.
  2. Two equation model.
  3. Reynolds stress equation model.
  4. Algebraic stress model
- Large eddy simulation.

3.4.1.1 Two-Equation models

Two equation turbulence models are one of the most common type of turbulence models. Models like the (*k*-ε) k-epsilon model and the (*k-ω)* k-omega model have become industry standard models and are commonly used for most types of engineering problems. Two equation turbulence models are also very much still an active area of research and new refined two-equation models are still being developed.

By definition, two equation models include two extra transport equations to represent the turbulent properties of the flow. This allows a two equation model to account for history effects like convection and diffusion of turbulent energy.

Most often one of the transported variables is the turbulent kinetic energy, *k*. The second transported variable varies depending on what type of two-equation model it is. Common choices are the turbulent dissipation, ε, or the specific dissipation, ω. The second variable can be thought of as the variable that determines the scale of the turbulence (length-scale or time-scale), whereas the first variable, k, determines the energy in the turbulence [17].

3.4.1.1.1 The k-ε model

k-ε model is the most popular two-equation model. The model had been developed by many turbulence researchers such as Chou and Davidov [16][13]. The first transported variable is turbulent kinetic energy, *k*. The second transported variable in this case is the turbulent dissipation, ε. According to J.J.M. Smits [18], there are three usual *k*-ε models:

- Standard *k*-ε model.
- RNG *k*-ε model.
- Realizable *k*-ε model.

The computations in the present thesis have mainly been carried out using Realizable *k*-ε model, (under the two -equation model category).

3.4.1.1.2 Realizable *k*-ε model

The last member of the $k - \varepsilon$ family is the Realizable k - ε model. It is a relative new turbulence model. It differs from the standard $k - \varepsilon$ model in two major ways. The first difference is the formulation of the turbulent viscosity and the second difference is the new transport equation for the dissipation rate [18].

In (3.8) and (3.9) the transport equations for both the kinetic energy and the dissipation rate are given.

$$U_j \frac{\partial}{\partial x_j}(\rho k) = \frac{\partial}{\partial x_j}\left(\left(\mu + \frac{\mu_t}{\sigma_k}\right)\frac{\partial k}{\partial x_j}\right) + G_k - \rho\varepsilon \qquad (3.8)$$

$$U_j \frac{\partial}{\partial x_j}(\rho \varepsilon) = \frac{\partial}{\partial x_j}\left(\left(\mu + \frac{\mu_t}{\sigma_\varepsilon}\right)\frac{\partial \varepsilon}{\partial x_j}\right) + \rho C_1 S_\varepsilon - \rho C_2 \frac{\varepsilon^2}{k+\sqrt{\nu\varepsilon}} \qquad (3.9)$$

Where

$$C_1 = \max\left[0.43, \frac{\eta}{\eta + 5}\right], \eta = S\frac{k}{\varepsilon}$$

Like the other $k - \varepsilon$ models, the turbulent viscosity is calculated using:

$$\mu_t = \rho C_\mu \frac{k^2}{\varepsilon}$$

The only difference is the constant C_μ

The closure coefficients:

$$C_2 = 1.9\,, \sigma_k = 1\,, \sigma_\varepsilon = 1.2$$

The Realizable k - ε model has shown substantial improvements over the standard k - ε model. Especially when the flow features include strong streamline curvature, vortices and rotation [18].

3.5 Compared Parameters

Average heat transfer coefficient, average Nusselt number and friction coefficient were approved as the basis for comparison of the performance of the different models.

3.5.1 Average Heat Transfer Coefficient

The average array heat transfer coefficient can be calculated by using the thermal energy difference between the flow inlet and the outlet, which is provided by the heat transfer summary in the output file of FLUENT at the end of the simulation, and by using the log mean temperature difference as below:

$$\bar{h} = \frac{\Delta Q}{A_{wh}\Delta T_{lm}} \qquad (3.10)$$

Where

A_{wh} is the heat transfer wetted surface area.

$$\Delta T_{lm} = \frac{(T_{wall} - T_{in}) - (T_{wall} - T_{out})}{\ln \frac{(T_{wall} - T_{in})}{(T_{wall} - T_{out})}} \quad (3.11)$$

Where the inlet bulk fluid temperature was constant and equal to 300K and the outlet bulk fluid temperature was calculated in the FLUENT program.

3.5.2 Nusselt Number

The Nusselt number is a dimensionless number that provides the ratio of the convective heat transfer over a surface that would occur by fluid motion to the corresponding conductive heat transfer and is a measure of the heat transfer ability. In our case more meaning makes the average Nusselt number which is given by the following relation:

$$N_u = \frac{\bar{h} D_h}{k} \quad (3.12)$$

3.5.3 Friction Factor

The dimensionless friction factor that was used was defined as follows.

$$f = \frac{\Delta P_{ave} D_h}{\frac{1}{2} \rho \bar{U}^2 L} \quad (3.13)$$

where ΔP_{ave} was the average pressure difference between the inlet and outlet sections of the heat exchanger. L is the total stream-wise length of the array.

CHAPTER 4

RESULTS

4.1 Computational Domain Descriptions

In this study, the heat exchanger domain consists of three connected channels: Entrance section, pin-fin section (CHE) and exit section. The compact heat exchanger domain consists of 10 rows of staggered drop shaped cross-pins with axes perpendicular to the flow, as shown in Figure (4.1). The main geometrical dimensions that characterize the heat exchanger are the pin height (*H*), the diameter of the cylindrical portion of the pin (*D*), the streamwise pin spacing (*X*), the spanwise pin spacing (*S*) and the pin-tail length (*L*). The streamwise pin spacing (*X*) and the spanwise pin spacing (*S*) were kept constant at a value equal to 50 mm. The heat exchanger is composed of a rectangular duct having 550 mm as length, 250 mm as width and *H* as height together with a bank of 45 solid pins that span the end walls.

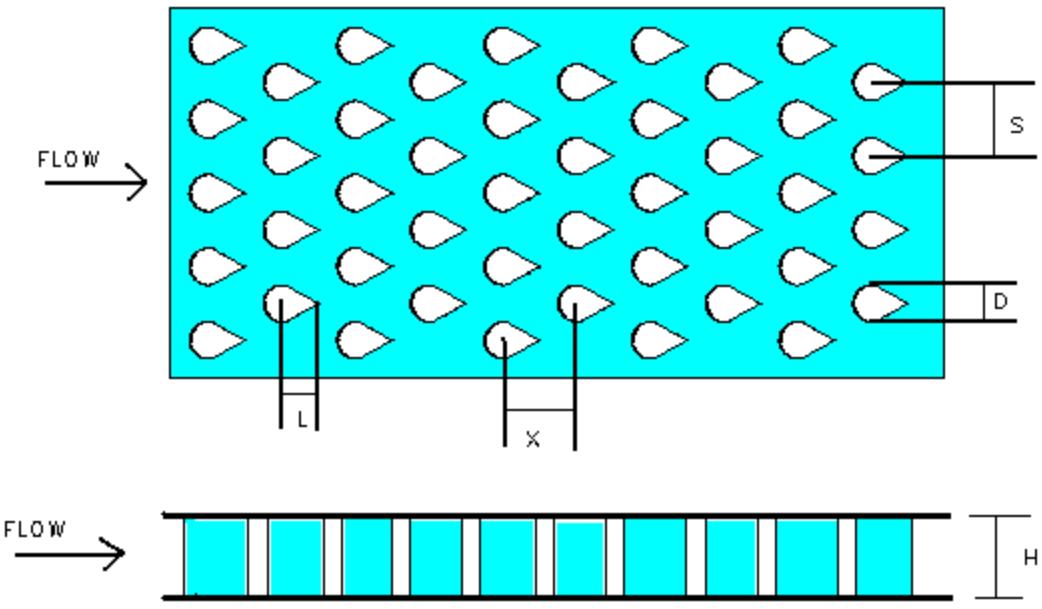

Figure (4.1): Pin fin section in the computational domain

4.2 Test Cases

Four drop shaped pin fin geometries having typical heat transfer wetted surface area were studied as shown in table (4.1) and figure (4.2). In all of these models, the streamwise pin spacing (*X*), the spanwise pin spacing (*S*) and the ratio of pin height to the cylindrical portion of the pin (*H/D*) remained constant while the other geometrical dimensions (*H*, *L* and *D*) were varied. The ratio (*H/D*) was kept constant at a value equal to the unity to be a short fin.

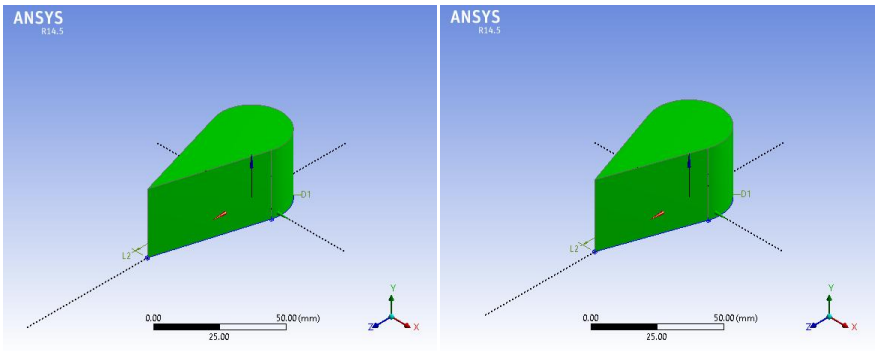

Case1 Case2

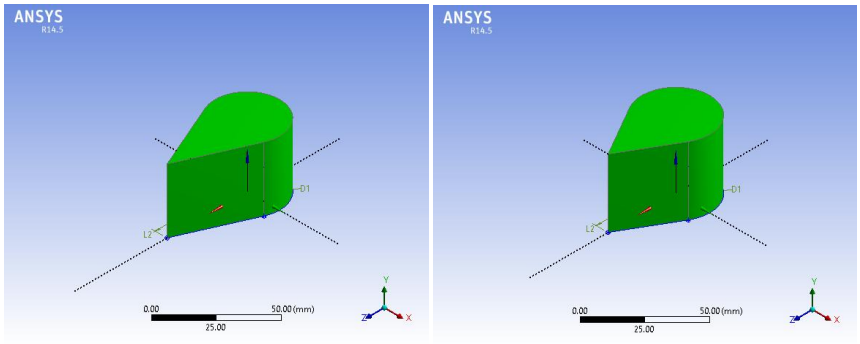

Case3 Case4

Figure (4.2): Different tested pin fins

Table (4.1): Geometrical dimension of the tested cases

cases	*H/D*	*L/D*	*D mm*	*L mm*	$A_{wf}mm^2$	$A_{wh}mm^2$	$V_{op}mm^3$	$D_h mm$	$A_{ave}mm^2$
1	1	1.75	31.55	55.22	426528.61	391819.3	2495611.48	23.40	4537.48
2	1	1.5	33	50	428119.30	391819.3	2609981.56	24.39	4745.42
3	1	1.25	34.85	43.57	430160.15	391819.3	2756719.37	25.63	5012.22
4	1	1	36.84	36.84	432338.50	391819.3	2913343.93	26.95	5296.99

4.3 Computational details

The CFD predictions were obtained by solving the three-dimensional Navier-Stokes equations with ANSYS Fluent 14.5.The computational model was specified to be three-dimensional, turbulence, and steady. Taking advantage of the symmetry planes in the heat exchanger, and in order to minimize the computational requirements and time, only one fourth of the heat exchanger was modeled, as shown in Figure (4.3). Based on this simplification, the model appears as shown in Figure (4.4). The SIMPLE algorithm is used to couple fluid pressure and velocity. The discretizations of momentum, turbulence, kinetic energy, turbulence dissipation rate, and energy equations were set to QUICK. The under relaxation factor for each iteration are for pressure = 0.3, momentum= 0.7, turbulence kinetic energy = 0.8, turbulence dissipation = 0.8 and energy = 1. The residual for converged solution of the continuity, component of velocity, turbulence kinetic energy and turbulence dissipation rate are below 10^{-3} while for energy is below 10^{-6}. To mesh the model, a uniform hexahedral element meshing was specified along the boundary and swept later to cover the entire model volume.

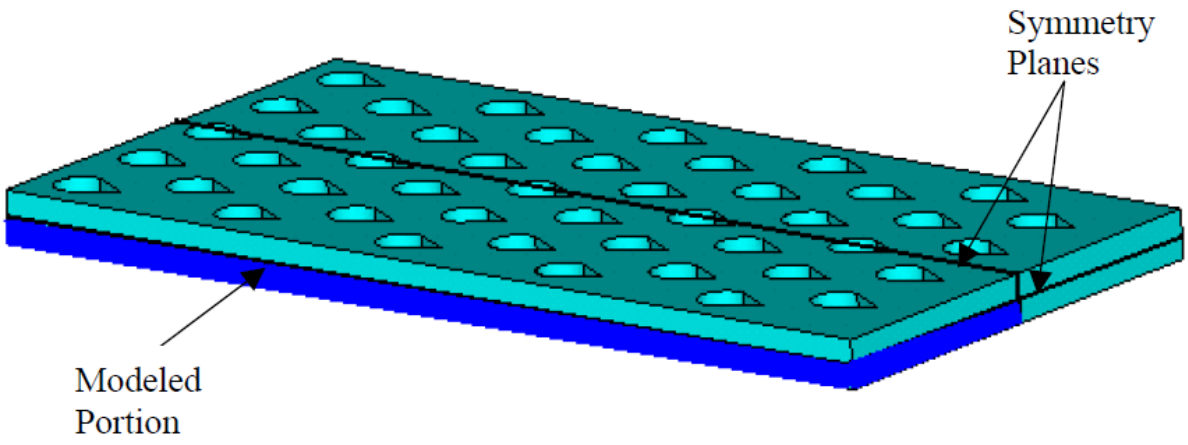

Figure (4.3): Symmetry planes and CHE model

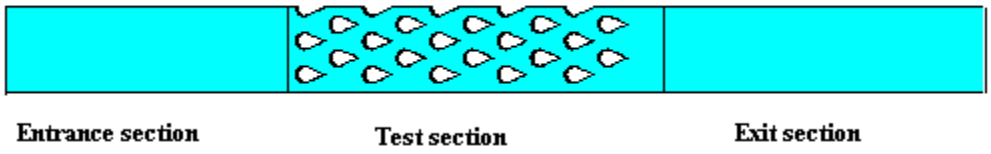

Figure (4.4): Finite element model

4.4 Boundary condition

4.4.1 Pins

The pins are treated as short pins *H/D*=1, eliminating the need to calculate the temperature distribution in the solid pins, and with very high thermal conductivity. The pins are therefore assumed to be isothermal with a uniform temperature of 312 K. The no slip condition was applied to the pin surfaces.

4.4.2 Upper and Lower Plates (End Wall)

The end wall was kept at a constant temperature of 312 K. Since it is a rigid boundary the no slip condition was applied leading to a zero velocity in the three directions, $U_x = U_y = U_z = 0$.

4.4.3 Entrance and Exit End Wall

The entrance and exit end walls were modeled as adiabatic walls with zero velocity in the three directions, $U_x = U_y = U_z = 0$.

4.4.4 Symmetry Walls

The symmetry walls are assumed to be adiabatic modeled with zero heat flux. The mid-height symmetry plane MHSP was given zero velocity in the z direction (U_z=0) and the mid-width symmetry plane MWSP was given a zero velocity in the y direction (U_y=0) thus preventing the flow from crossing the boundary but yet allowing a velocity profile to develop. The inlet and exit symmetry walls have the same features as in the test section.

4.4.5 Side Wall

The sidewall was modeled to be adiabatic with zero heat flux. The no slip condition was applied and zero velocity in the tree direction ($U_x = U_y = U_z$=0) was used. The inlet and exit sidewalls has the same properties as the same properties as the test section ones.

4.4.6 Inlet

To simplify the model only the fluid (incompressible ideal gas - air) was modeled. The inlet air temperature was set to 300 K. The inlet velocity depends on the chosen Reynolds number, which was set based on the wetted surface area.

Figures (4.5) give a clear idea of the boundary conditions implemented.

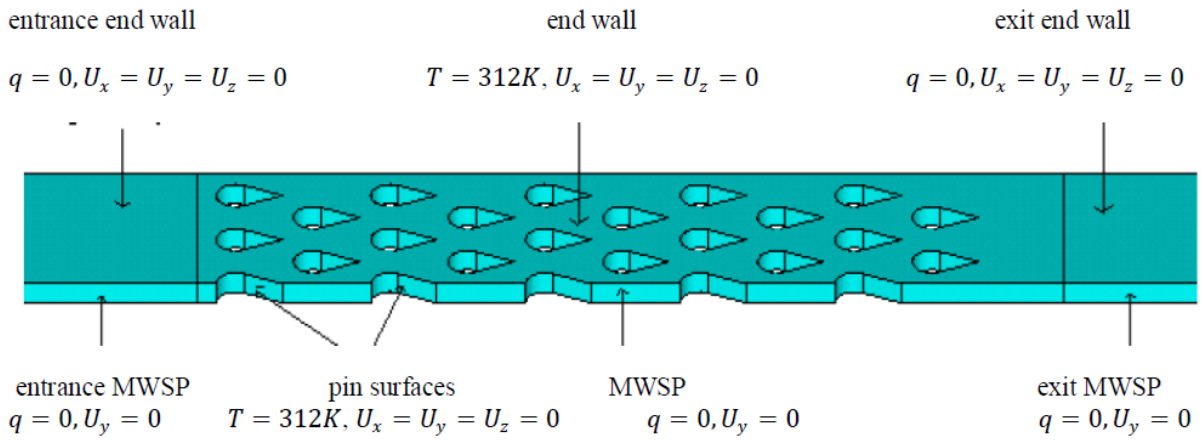

Figure (4.5): Models view with boundary conditions

4.5 Grid Independence Study

A grid-independent solution exists when the solution no longer changes with further grid refinement. After each solution convergence on a computational model, a new grid was constructed using a higher cell density. The solution resulting from the new mesh was compared to the solutions resulting from the previous mesh. This process continued until a grid independent solution was obtained. Figure (4.6) and Figure (4.7) shows the prediction of heat transfer flux and outlet temperature solution for several different meshes. Thus, to achieve grid independence the computed heat transfer flux and outlet temperature had to reach less than one percent variation (1%) between subsequent grid refinements. The grid independence study was performed with the case *L/D=1.5* , case No.2.

Table (4.2) shows grid independence study results for the last three mesh refining. The results indicated that the last mesh refining which had element size of 1.25 mm is the best one because the heat flux error and the outlet temperature error was the smallest one.

Table (4.2): Grid independence for model with hexahedral elements

Parameter	Grid 1	Grid 2	Grid 3
Elements number	430183	466570	536368
Nodes number	490686	531146	606435
ΔQ (W)	82.28	82.74	82.88
Error (%) for ΔQ	0.74	0.56	0.17
T_{out} (K)	305.59	305.62	305.60
Error (%) for T_{out}	0.02	0.01	0.00

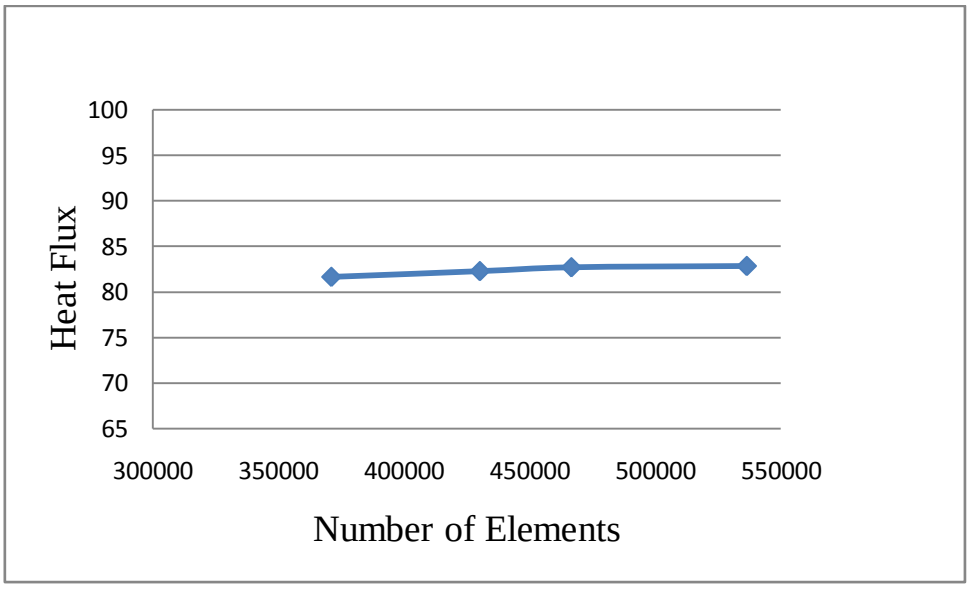

Figure (4.6): The variation of Heat Transfer Flux with various mesh

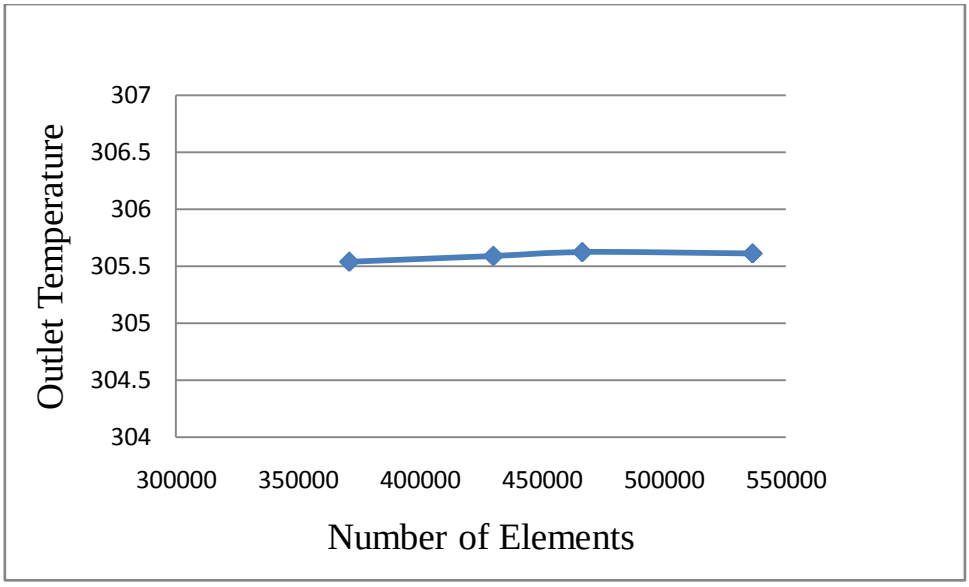

Figure (4.7): The variation of Outlet Temperature with various mesh

4.6 Validation

Today Computational Fluid Dynamics (CFD) is used for simulating flow in many engineering applications. Validation is the primary mean to assess accuracy and reliability in computational simulations. Validation is defined as a process for assessing modeling uncertainty by using benchmark experimental data [20]. In this work CFD results were compared with experimental data of Jeffrey W. Summers [12], the work concentrated on the empirical characterization of a staggered array pin fin compact heat exchanger placed in a modular, rectangular wind tunnel. A full analysis of the heat transfer and pressure drop behavior was conducted on drop shaped pin fin. The study was based on airflow over a range of low Reynolds numbers in the laminar and low turbulent flow, as well as higher turbulent flow regimes.

A Comparison between Jeffrey W. Summers [12] experimental data and CFD prediction is carried out to validate the numerical results presented in this thesis. Figures (4.8), (4.9) and (4.10) show friction coefficient, average heat

transfer coefficient and Nusselt number curves which presented the variation of them against Reynolds number. The first curve was measure by experimental data and the other one predicted by CFD simulation. The observation that numerical results and experimental data curves had the typical trends. The primary points in the both carves had the same values but the deviation increased as Reynolds number increasing. The maximum deviation of friction coefficient, heat transfer coefficient and Nusselt number was 33.3%, 31.8% and 31.1% respectively. This deviation could be attributed to the computational errors. Since a normal computer (Laptop, Intel Pentium) was used in the current simulation, for more accurate solution super computer must be used.

The results presented in this validation indicate that CFD may indeed provide a practical method of analyzing heat exchanger designs.

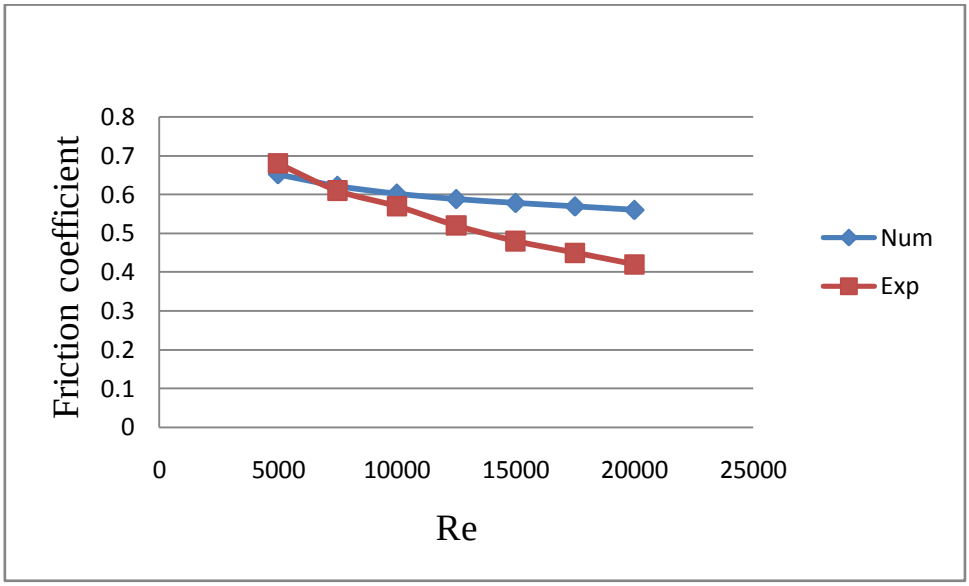

Figures (4.8): Friction coefficient variation against Reynolds number

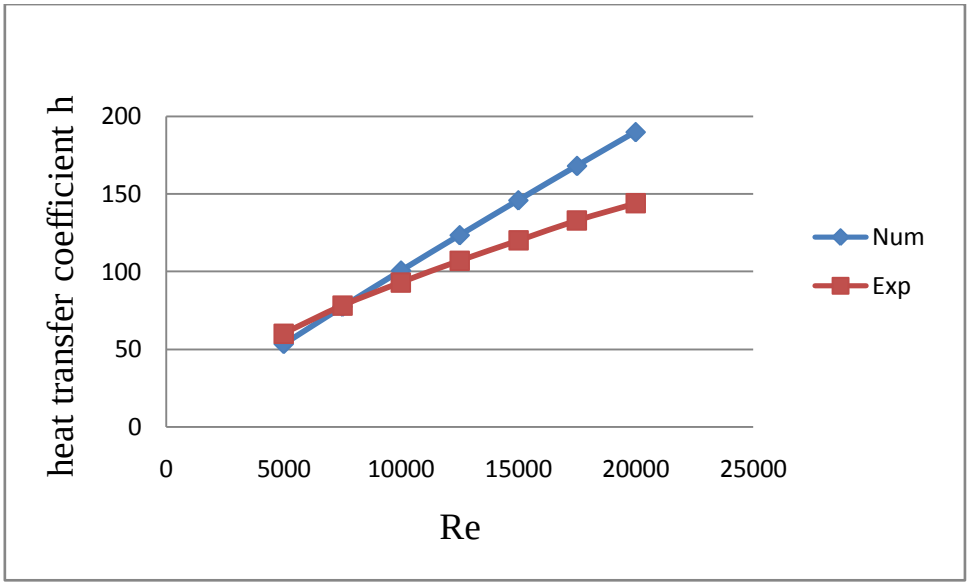

Figures (4.9): Heat transfer coefficient variation against Reynolds number

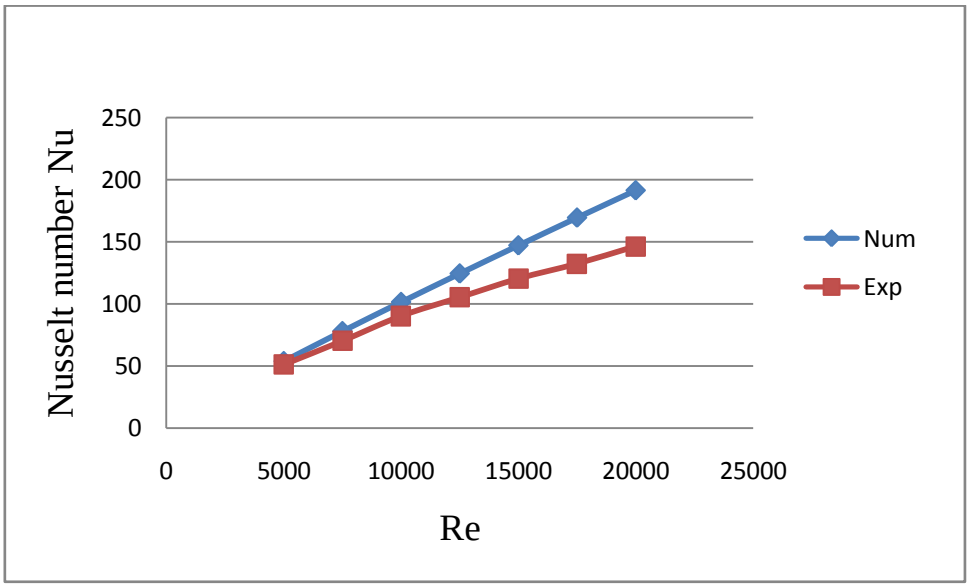

Figures (4.10): Nusselt number variation against Reynolds number

4.7 Results and Discussions

This focus of this study was on investigating the heat transfer and pressure losses inside a drop-shaped pin fin heat exchanger. Average heat transfer coefficient, average Nusselt number and friction coefficient were approved as the basis for comparison of the performance of the different models.

4.7.1 Average heat transfer coefficient

The heat transfer coefficient is one of the most critical and interesting of the examined parameters. The heat transfer coefficient was calculated based on the heat transfer wetted surface area as well as system heat transfer rate flow and bulk differential log mean temperature. Figure (4.11) displays the average heat transfer coefficient versus Reynolds number results for the different models in the turbulent flow region. From the figure (4.11) for different tail length *L/D* =1.75, 1.5, 1.25 and 1 the results indicate that in general average heat transfer coefficient is increase with Reynolds number and the variations in the tail length of drop shaped pin fins don't affect heat transfer coefficient because the heat transfer wetted area or surface wetted area remain constant for the four cases. That means heat transfer coefficient don't affect by the aerodynamics of pin fin.

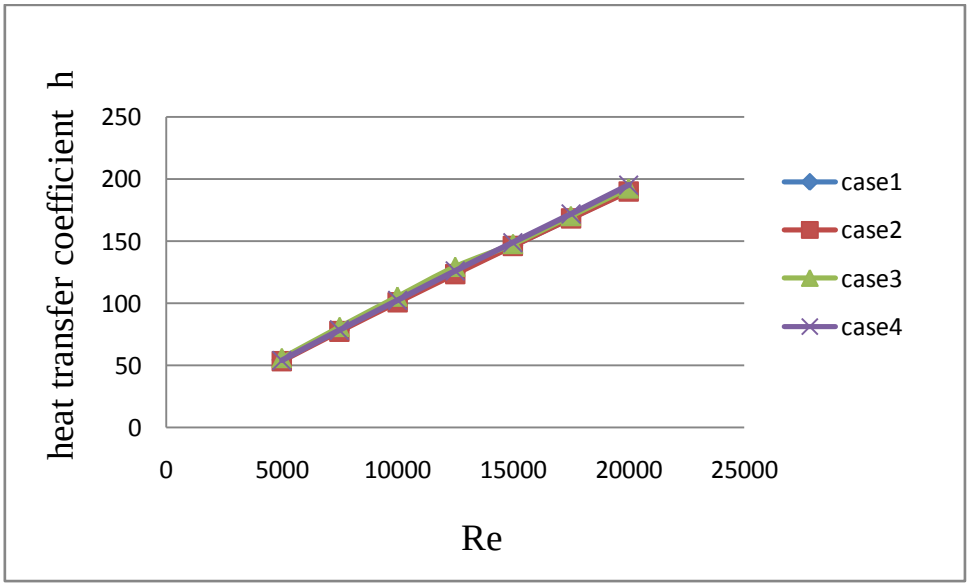

Figures (4.11): Heat transfer coefficient versus Reynolds number.

4.7.2 Nusselt number

The Nusselt number is a dimensionless temperature gradient that details the convective heat transfer. The larger the Nusselt number the more productive the convective heat transfer process is. The Nusselt number is proportional to

the heat transfer coefficient and hydraulic diameter and inversely proportional to the thermal conductivity of the system. Figure (4.12) shows how the Nusselt number varied with the Reynolds number in the turbulent range. With the Nusselt number being directly proportional to the heat transfer coefficient the expected results should have been similar to the heat transfer coefficient data. The change in order is attributed to the increase in hydraulic diameter, see table (4.1). From figure (4.12), case number four which has the greatest hydraulic diameter achieved the highest heat transfer performance and case number one achieved the lowest one.

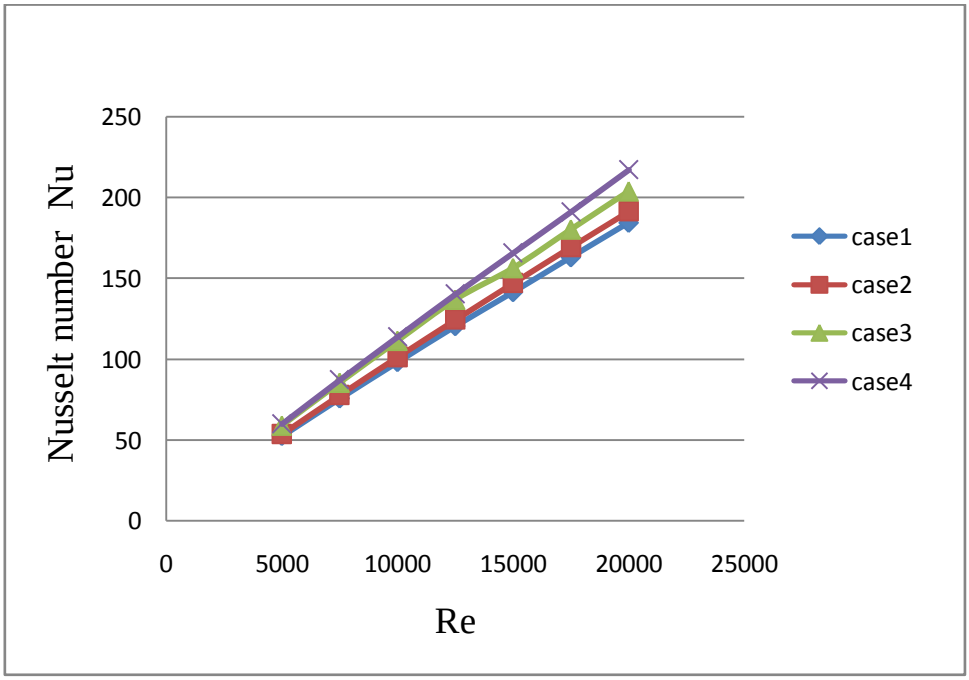

Figures (4.12): Nusselt number versus Reynolds number.

4.7.3 Friction Coefficient

The friction factor is an important parameter because it tells how much power was required to achieve the heat transfer results. Friction factor is directly proportional to the differential pressure across the CHE and hydraulic diameter, while being inversely proportional to density and average fluid velocity. Figure

(4.13) show the results of friction factor versus Reynolds number in the turbulent region.

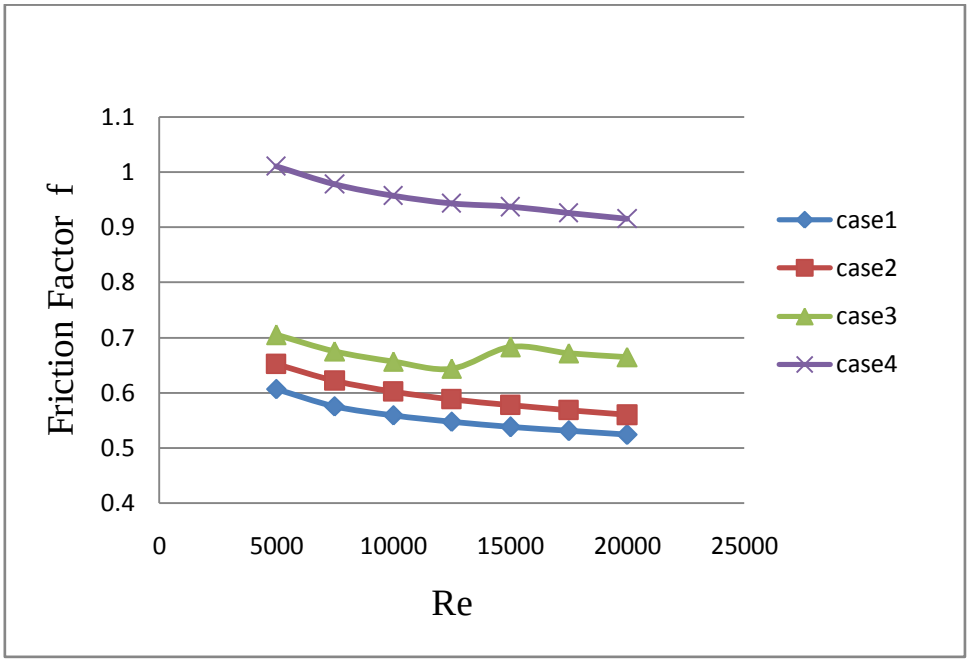

Figures (4.13): Friction coefficient versus Reynolds number.

As can be derived from the graphs, as pin fin tail were shorter (small *L/D*) the differential pressure across the heat exchanger increased causing friction factor to increase. In addition since friction factor is directly proportional to the hydraulic diameter this mean the largest hydraulic diameter the greatest friction factor so that case number four has the highest friction factor carve and case number one has the lowest one.

Other reason to increasing pressure losses is boundary layer separation. Because of the drops overlapping, the flow was forced to reattach after separation so that it cannot be clear except in the last row, so enlargement for domain end was needed. Refer to figure (4.14), (4.15), (4.16) and (4.17) taking Reynolds number equal to 5000 as a sample the observation that the drop shaped tail length was really affect separation process since the model which

has the longest pins tail forces separation to delay and if the fins tail is shorter separation will occur early.

In figure (4.17) case 4, the flow result indicate that there is a clear vortices in addition to flow separation and this resulting in abnormal increasing to friction coefficient comparing to other models.

From figure (4.13) for case 3 the friction coefficient graph experience a sudden jump at Reynolds number 15000, and that could be attributed to the variation in the flow field, see figures (4.18) and (4.19)

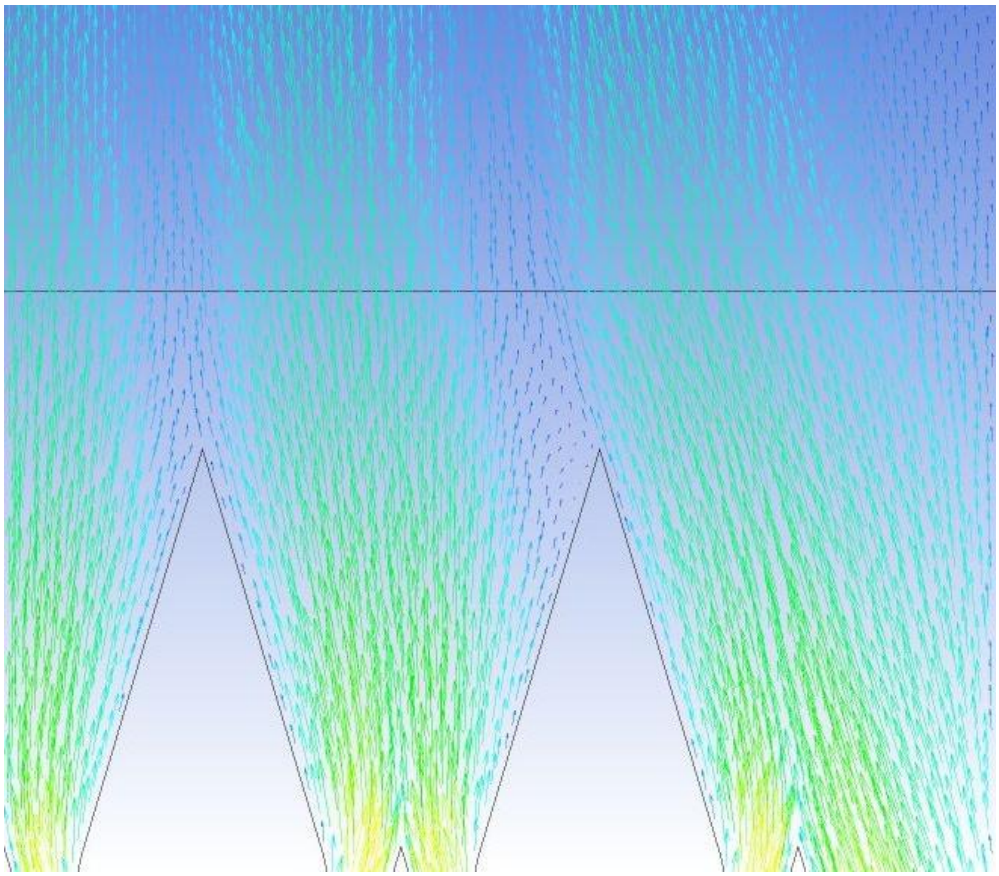

Figure (4.14): Velocity vectors of the last row in case1 (L/D=1.75).

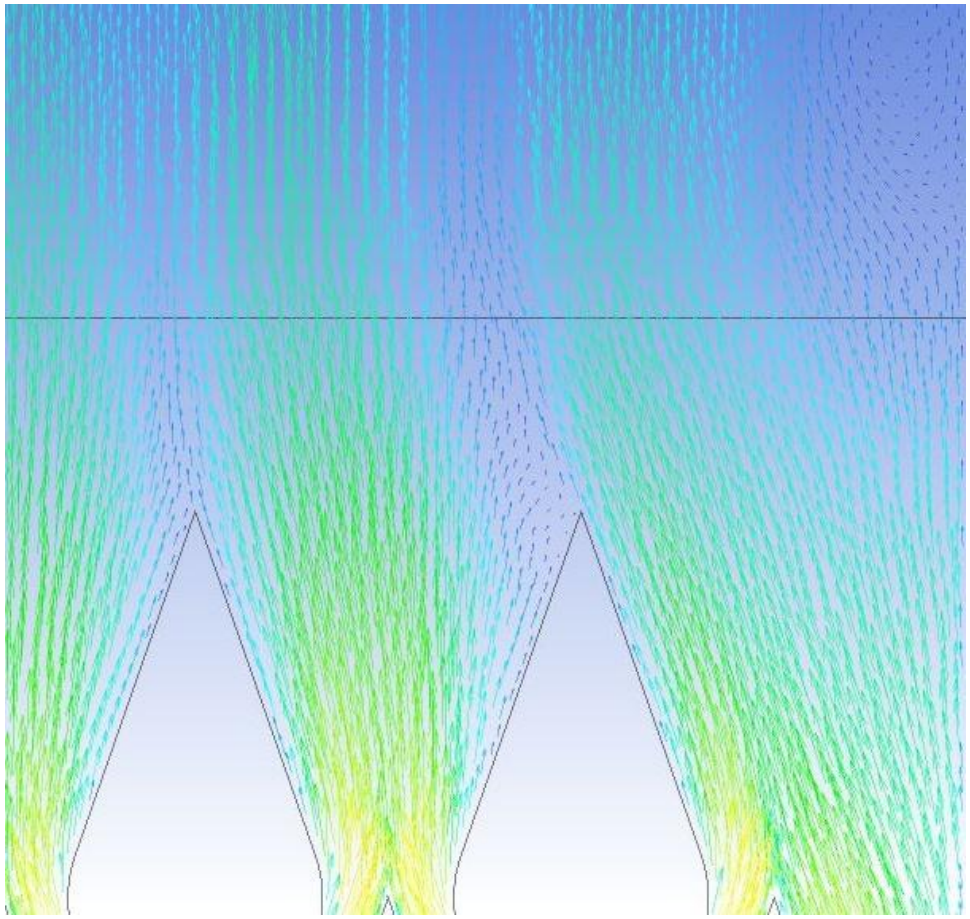

Figure (4.15): Velocity vectors of the last row in case2 (L/D=1.5).

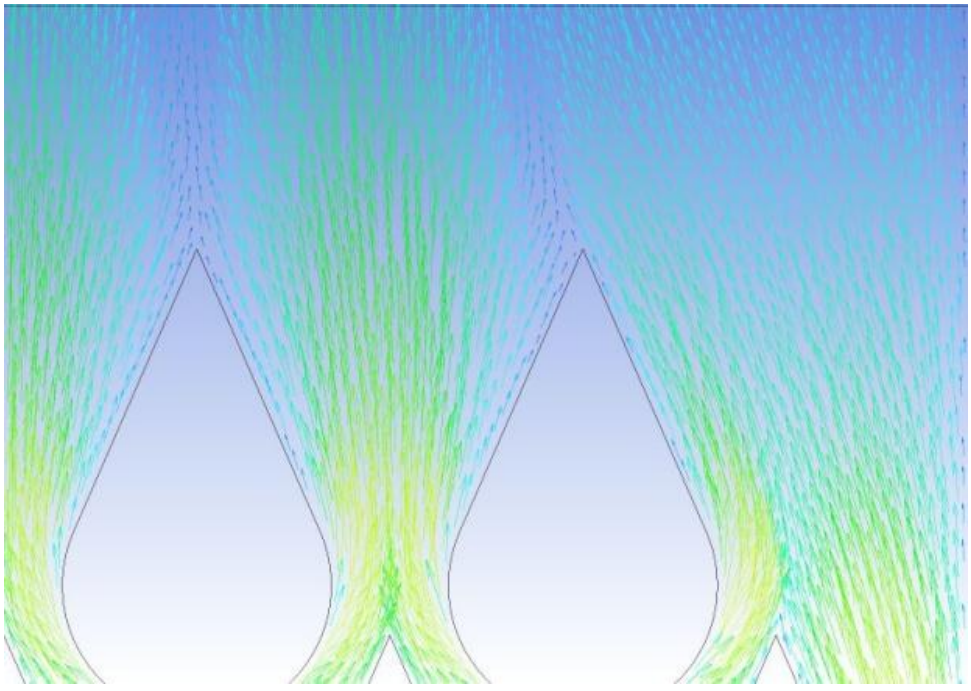

Figure (4.16): Velocity vectors of the last row in case3 (L/D=1.25).

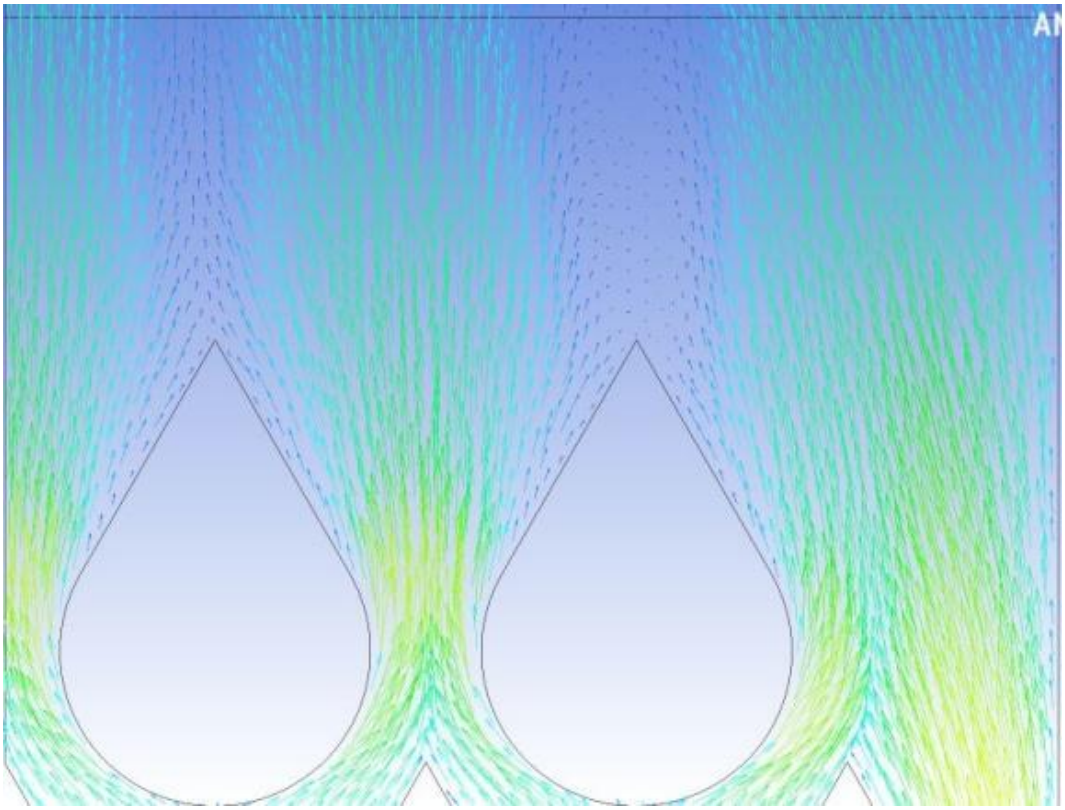

Figure (4.17): Velocity vectors of the last row in case4 (L/D=1).

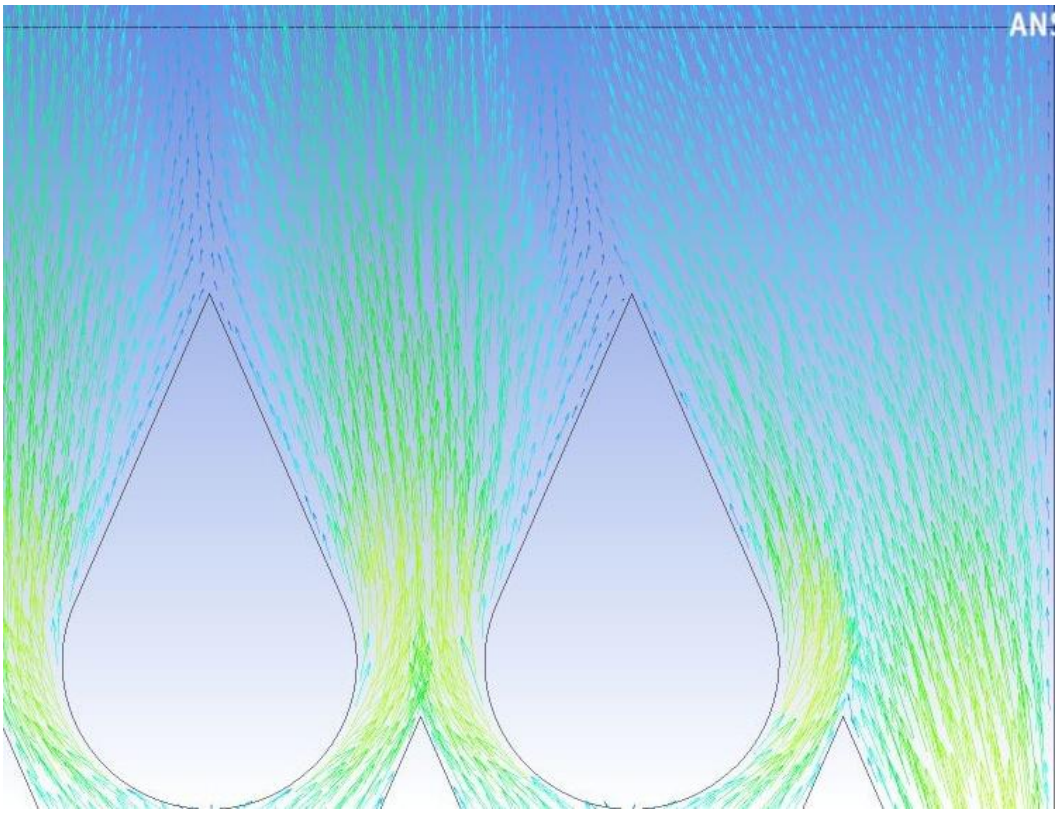

Figure (14.18): Velocity vectors for case 3 at Reynolds number 12500

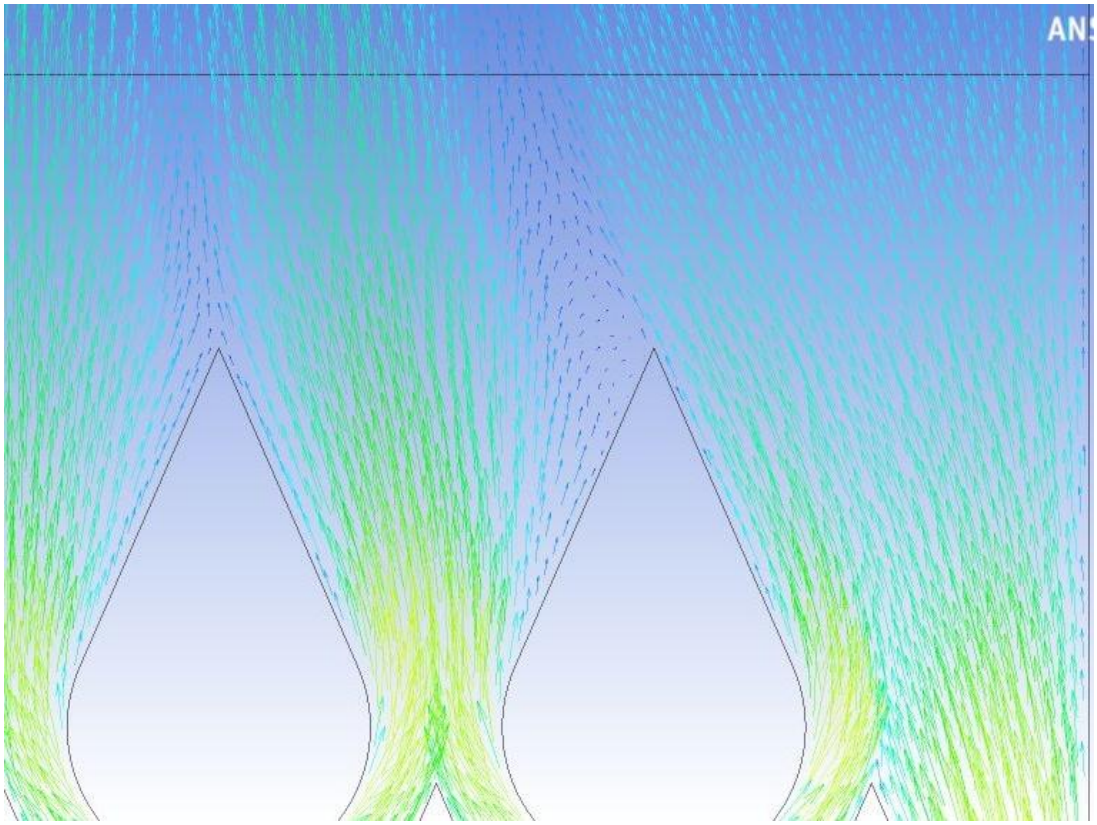

Figure (4.19): Velocity vectors for case 3 at Reynolds number 15000

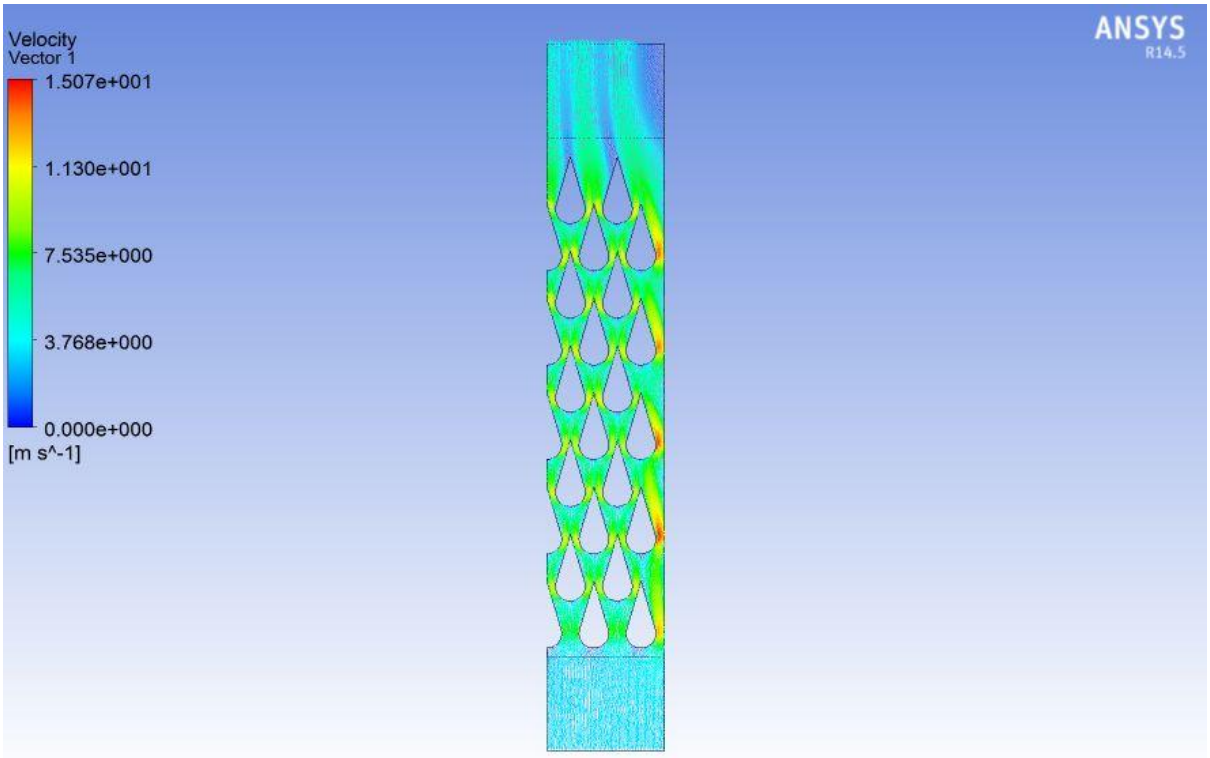

Figure (4.20): Velocity vector for case1

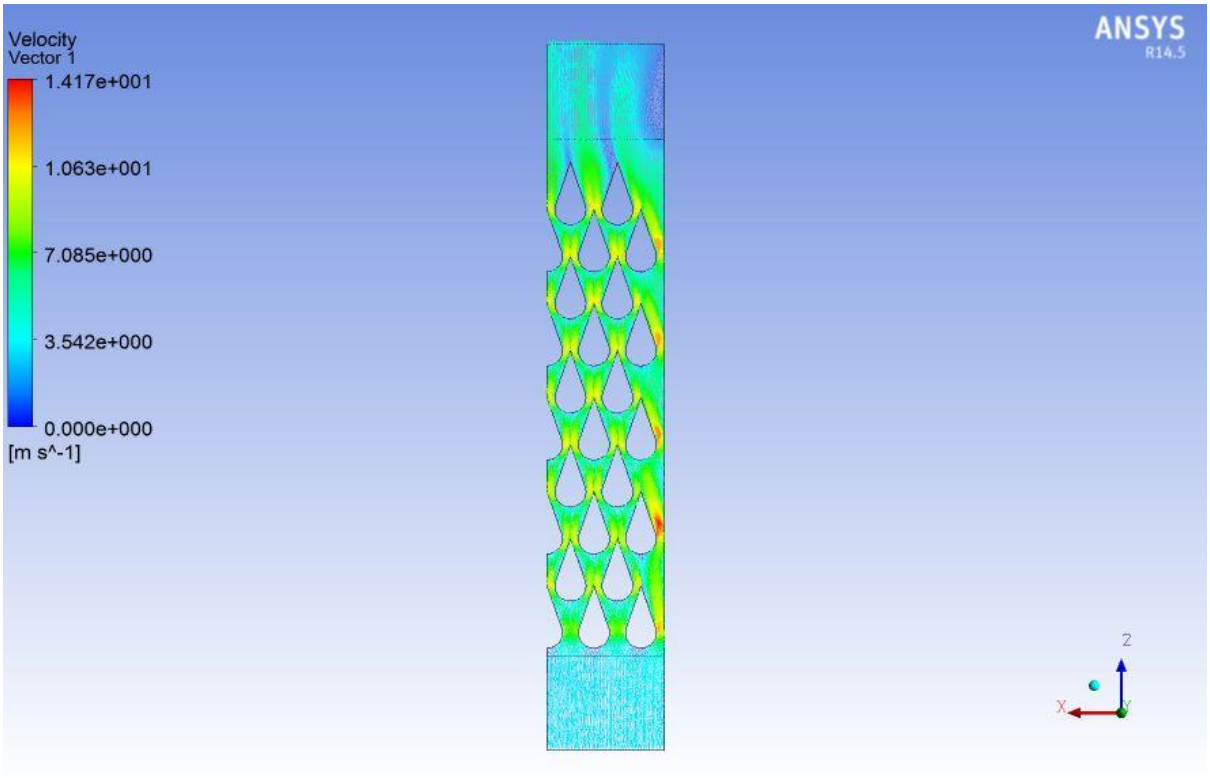

Figure (4.21): Velocity vector for case2

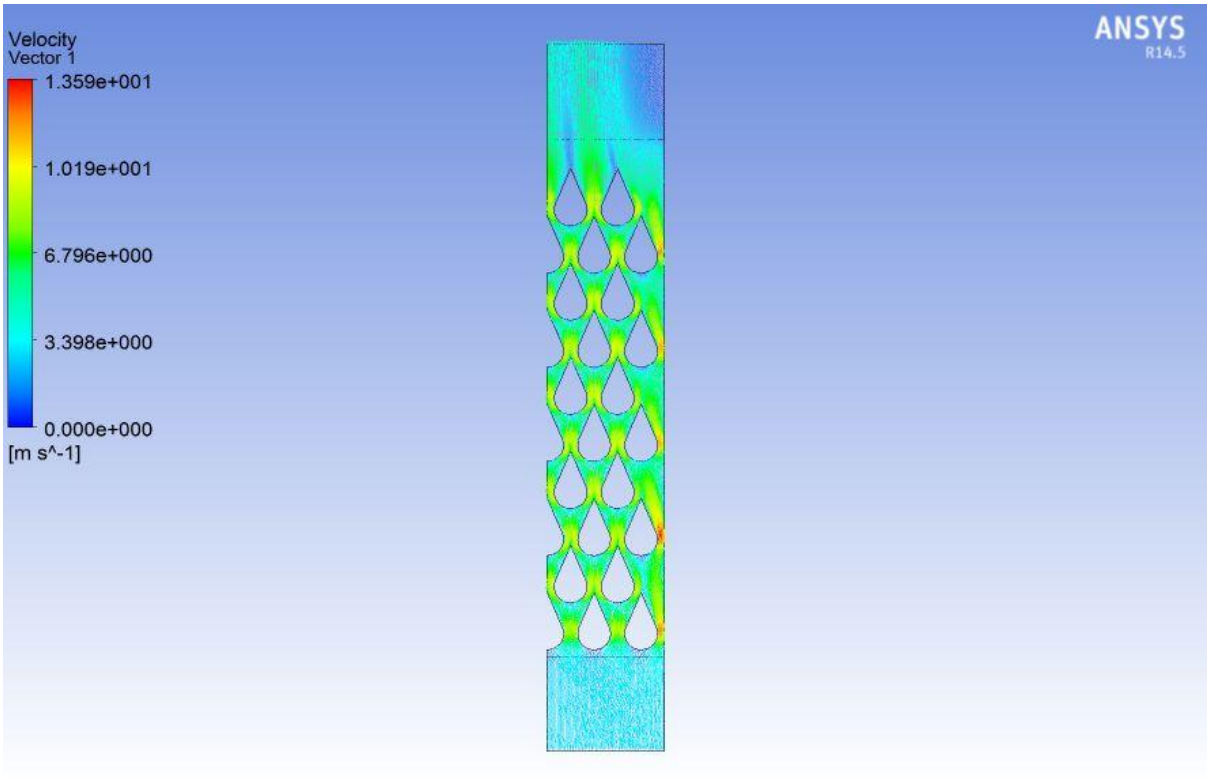

Figure (4.22): Velocity vector for case3

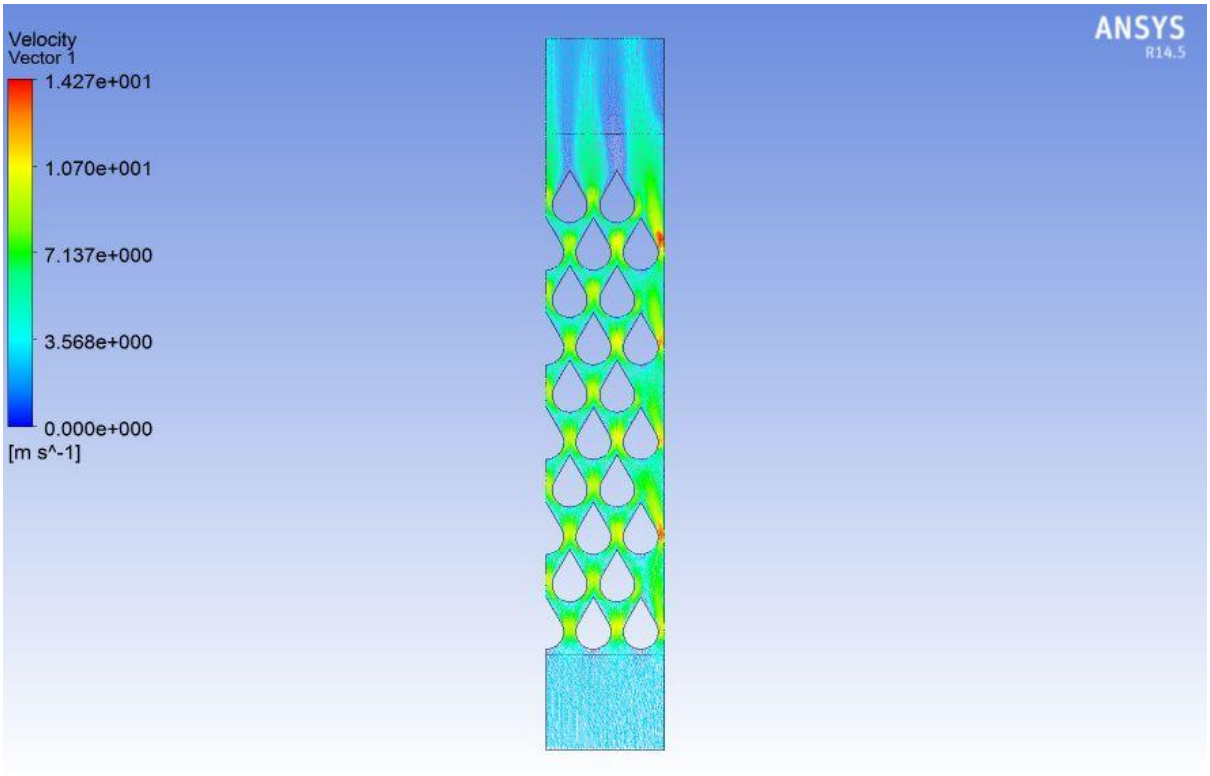

Figure (4.23): Velocity vector for case4

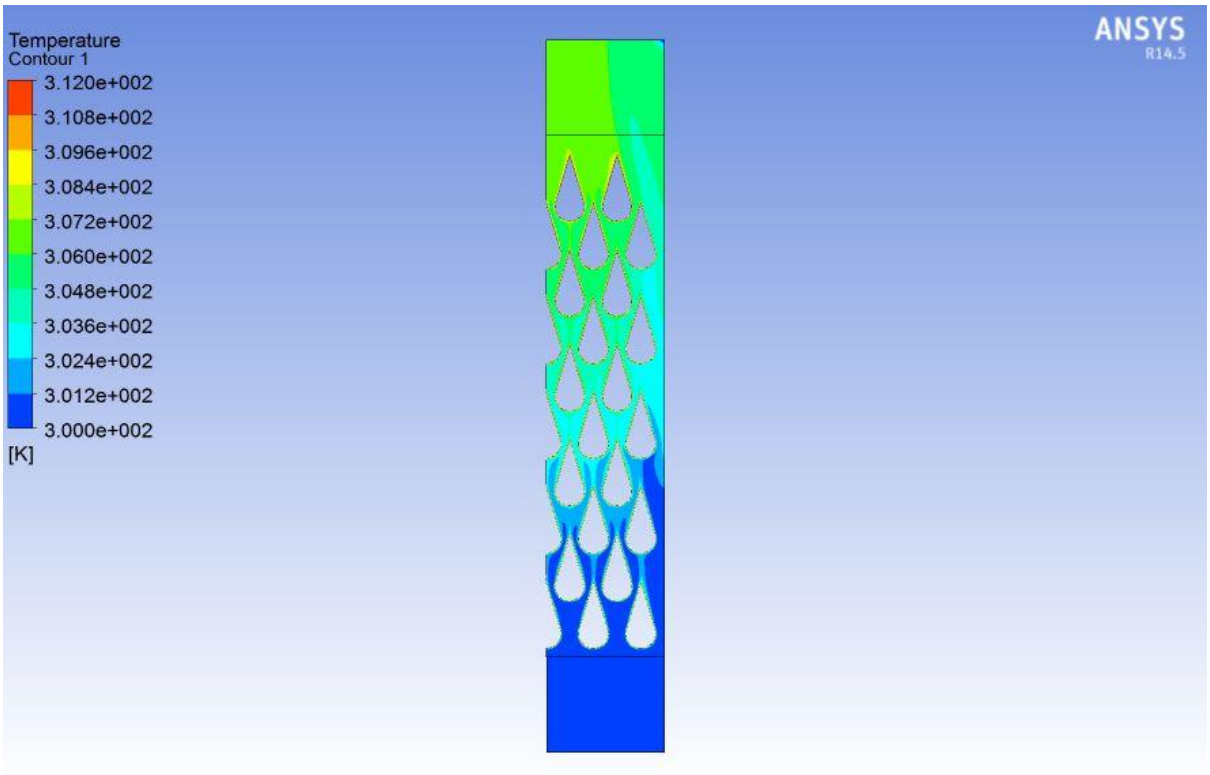

Figure (4.24): Temperature contour for case1

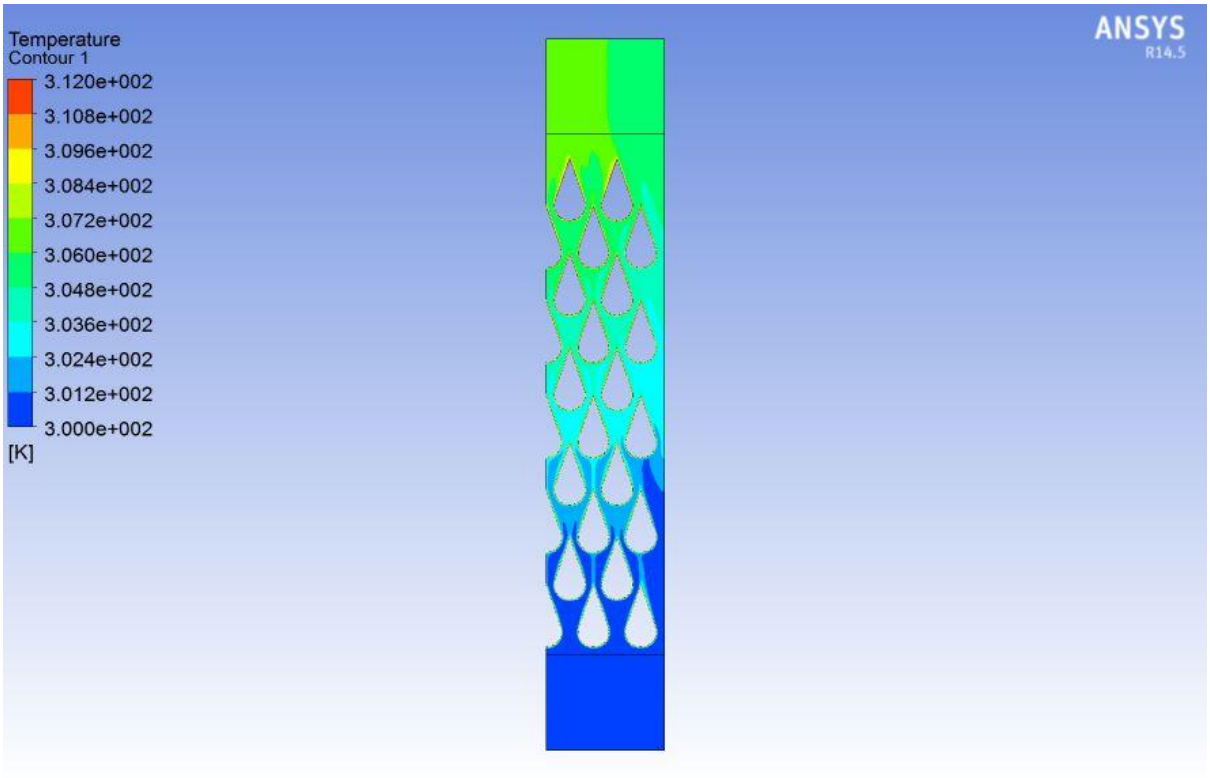

Figure (4.25): Temperature contour for case2

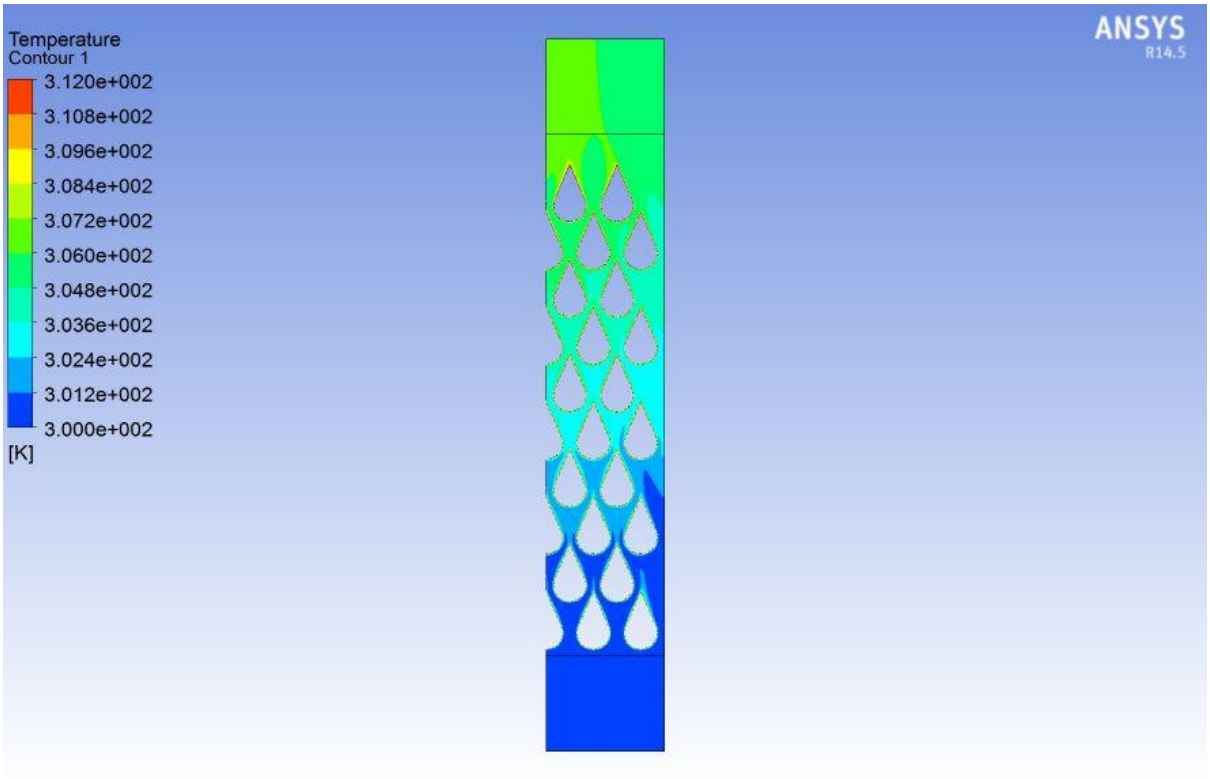

Figure (4.26): Temperature contour for case3

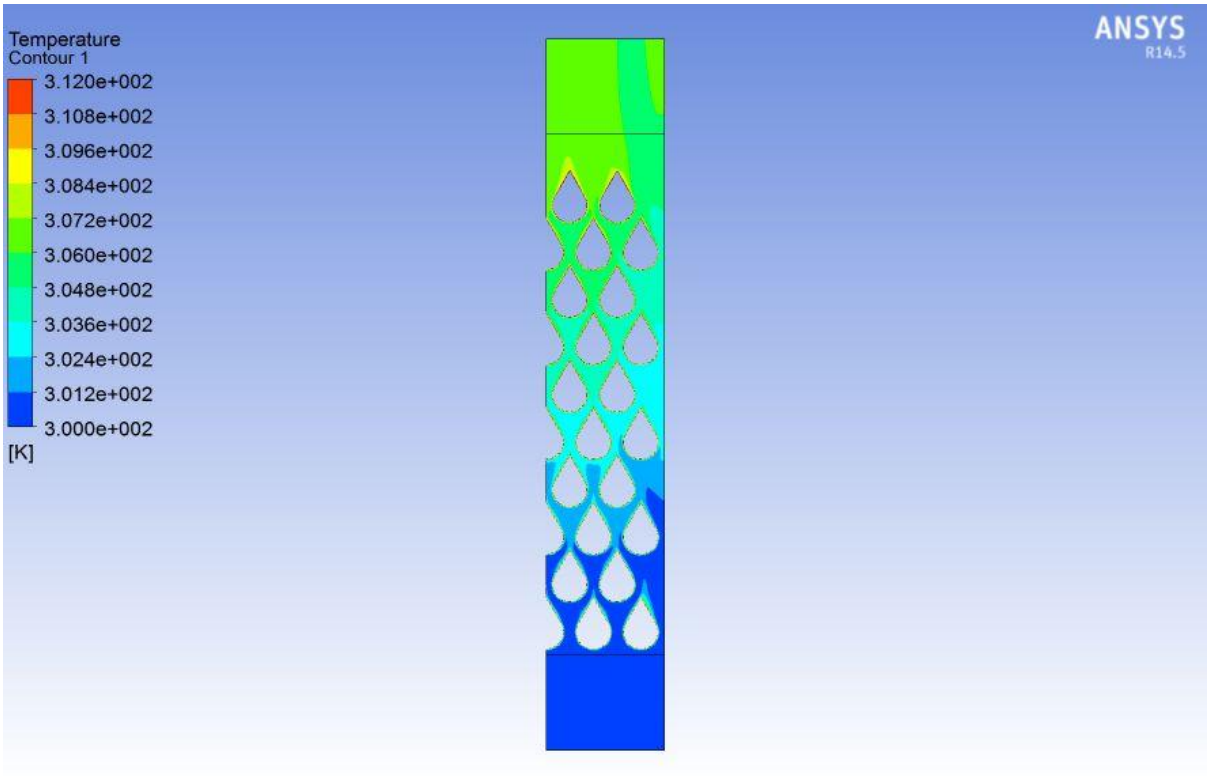

Figure (4.27): Temperature contour for case4

Figures (4.20), (4.21), (4.22) and (4.23) show velocity vector for different cases at Reynolds number 5000 as a sample. The results indicated that while pin tail decreasing pins overlapping decreased. The lost of pin overlapping as can be seen from the above figures causing the lost of nozzle effect leading to more power consumption to accelerate air flow. The maximum velocity which can be achieved across heat exchanger gained by case No.1 due to the great pin overlapping. The observation that the maximum velocity across the heat exchanger decreased with decreasing of the ratio *L/D.*

Figures (4.24), (4.25), (4.26) and (4.27) show temperature contour for different cases at Reynolds number 5000 as a sample. The results indicated that the maximum outlet temperature belonged to case No.4 and that could be attributed to the air velocity across the heat exchanger. Since air velocity in case No.4 was the slowest one that's mean air was spent a long time in heat exchanger compared to the other cases to be hotter.

CHAPTER 5

CONCLUSIONS & RECOMMENDATIONS

5.1 Conclusions

A 3-D numerical simulation was conducted to evaluate the performance of a compact heat exchanger made of different dimensions drop shaped pin fins. The task was to vary the drop tail length and identified the best drop dimensions capable of increasing the heat transfer and decreasing pressure drop or losses (frictional losses) across heat exchanger while keeping the same heat transfer wetted surface area. A comparison between the drops was conducted to evaluate the improvement in heat transfer and pressure drop.

The numerical results for the for four cases L/D 1, 1.25, 1.5 and 1.75 indicated that the variations in pin tail length was not highly affect heat transfer but it definitely highly affect frictional losses or pressure drop. The numerical results indicated that the highest friction coefficient curve was belonged to the shortest pin tail length fins and the lowest friction coefficient carve was belonged to the tallest pin tail length fins. In other word as the pin tail length is increasing the frictional loss decreasing. Also the highest Nusselt number carve was belonged to the shortest pin tail length fins and the lowest Nusselts number carve was belonged to the tallest pin tail length fins. So that the optimum pin fin dimension is case No.1, L/D=1.75, because it achieved the minimum frictional losses for the same heat transfer coefficient.

5.2 Recommendations

- This thesis could be considered as an introductory study to illustrate the utility of computational flow analysis in the analysis and optimization of heat transfer and pressure drop in compact heat exchanger with different shapes of pin fin. Further and more complete studies are needed to quantify the design parameters for pin fins.
- Investigating other pin shapes that may have better performance than drop pins.
- The increasing of the ratio H/D could have a big influence on the wetted surface area and as a result a big influence on the heat transfer rate. So investigating the influence of H/D could be the next step in a future study.

APPENDIX

EQUATIONS

1. Flow Wetted Surface Area

$$A_{wf} = 2\left[LW + LH - N_p\left(\frac{\pi D^2}{4}\left(\frac{\pi + 2\theta}{2\pi}\right) + \frac{D}{2}lcos\theta\right)\right] +$$

$$N_p H\left[\frac{D}{2}(\pi + 2\theta) + 2lcos\theta\right]$$

2. Heat Transfer Wetted Surface Area

$$A_{wh} = 2\left[LW - N_p\left(\frac{\pi D^2}{4}\left(\frac{\pi + 2\theta}{2\pi}\right) + \frac{D}{2}lcos\theta\right)\right] +$$

$$N_p H\left[\frac{D}{2}(\pi + 2\theta) + 2lcos\theta\right]$$

3. Open Volume

$$V_{op} = LWH - N_p H\left[\left(\frac{\pi D^2}{4}\left(\frac{\pi + 2\theta}{2\pi}\right) + \frac{D}{2}lcos\theta\right)\right]$$

4. Hydraulic Diameter

$$D_h = \frac{4V_{op}}{A_{wf}}$$

5. Average Flow Area

$$A_{\boldsymbol{ave}} = \frac{V_{op}}{L}$$

6. Reynolds number

$$Re = \frac{\dot{m} D_h}{\mu A_{ave}} = \frac{\rho \bar{U} D_h}{\mu}$$

$$\bar{U} = \frac{\dot{m}}{\rho A_{ave}}$$

7. Outlet Temperature

$$T_{out} = T_{in} + \frac{Q}{\dot{m} C_p}$$

References

[1] Frank Kreith, Raj M. Manglik, Mark S. Bohn "Principles of HEAT TRANSFER" Cengage Learning, 2011

[2] Naser Sahiti "Thermal and Fluid Dynamic Performance of Pin Fin Heat Transfer Surfaces"PhD Thesis, Erlangen University, 2006

[3] M. Udaya kumar, M. Manzoor Hussian, Md. Yousaf Ali "Review of Heat Transfer Enhancement Techniques in Square Ducts with Inserts" International Journal of Emerging Technology and Advanced Engineering, volume 3, 2013

[4] Ramesh K. Shah and Dušan P. Sekulic "Fundamentals of Heat Exchanger Design" John Wiley & Sons 2003

[5] C. L. Chapman and Seri Lee "Thermal Performance of an Elliptical Pin Fin Heat Sink" Tenth IEEE SEMI-THERM,1994

[6] Ambeprasad.S.Kushwaha, Prof. Ravindra Kirar, "Comparative Study of Rectangular, Trapezoidal and Parabolic Shaped Finned Heat sink" paper, IOSR Journal of Mechanical and Civil Engineering 2013

[7] Yoav Peles , Ali Kosar, Chandan Mishra, "Forced convective heat transfer across a pin fin micro heat sink" paper, International Journal of Heat and Mass Transfer 2005

[8] Michael E. Lyall, "Heat Transfer from Low Aspect Ratio Pin Fins" MSc Thesis, State University 2006

[9] Fengming Wang, JingzhouZhangb, SuofangWang, paper "Investigation on flow and heat transfer characteristics in rectangular channel with drop-shaped pin fins" paper, Propulsion and Power Research 2012

[10] Hamid Nabati "Optimal Pin Fin Heat Exchanger Surface" MSc Thesis, Mälardalen University 2008

[11] Jihed Boulares "Numerical and Experimental Study of the Performance of a Drop-Shaped Pin Fin Heat Exchanger"2003

[12] Jeffrey W. Summers "an Empirical Study of a Pin Fin Heat Exchanger in Laminar and Turbulent Flow" MSc Thesis Naval Postgraduate School 2003

[13] H. K. Versteeg and W. Malalaskera, "Introduction to Computational Fluid Dynamics - The Finite Volume Method," Longman Scientific & Technical, Harlow, England, Second Edition,2007

[14] Khobib Abdelhafeiz Mohamed, "Numerical Study of Application of Shape Memory Alloy in Louvered Fins Radiators" MSc thesis, UofK 2013

[15] Timothy Barth and Mario Ohlberger, "Finite volume methods: foundation and analysis" Encyclopedia of Computational Mechanics 2004

[16] Obai Younis Taha, "Formulation, Implementation and Testing of $k-\omega-v^2-f$ Model in an Asymmetric Plane Diffuser" MSc thesis, Chalmers University of Technology, Sweden, 2004

[17] http://www.cfd-online.com/

[18] J.J.M. Smits "Modeling of a Fluid Flow in an Internal Combustion Engine" Eindhoven University of Technology,2006

[19] Sotirios Dimas "A CFD Analysis of the Performance of Pin-Fin Laminar Flow Micro/Meso Scale Heat Exchangers" MSc Thesis, Naval Postgraduate School 2005

[20] W. L. Oberkampf and T. G. Trucano "Validation Methodology in

Computational Fluid Dynamics" Sandia National Laboratories, 2000